Impacts of Low-Frequency Internal Climate Variability and Greenhouse Warming on El Niño–Southern Oscillation⚘

BENJAMIN NG,[a,b] WENJU CAI,[a,b,c,d] TIM COWAN,[e,f] AND DAOHUA BI[b]

[a] *Centre for Southern Hemisphere Oceans Research, CSIRO Oceans and Atmosphere, Hobart, Tasmania, Australia*
[b] *CSIRO Climate Science Centre, Aspendale, Victoria, Australia*
[c] *Key Laboratory of Physical Oceanography, Institute for Advanced Ocean Studies, Ocean University of China, Qingdao, China*
[d] *Qingdao National Laboratory for Marine Science and Technology, Qingdao, China*
[e] *Centre for Applied Climate Sciences, University of Southern Queensland, Toowoomba, Queensland, Australia*
[f] *Bureau of Meteorology, Melbourne, Victoria, Australia*

ABSTRACT: El Niño–Southern Oscillation (ENSO) is the dominant mode of interannual climate fluctuations with wide-ranging socioeconomic and environmental impacts. Understanding the eastern Pacific (EP) and central Pacific (CP) El Niño response to a warmer climate is paramount, yet the role of internal climate variability in modulating their response is not clear. Using large ensembles, we find that internal variability generates a spread in the standard deviation and skewness of these two El Niño types that is similar to the spread of 17 models from phase 5 of the Coupled Model Intercomparison Project (CMIP5) that realistically simulate ENSO diversity. Based on 40 Community Earth System Model Large Ensemble (CESM-LE) and 99 Max Planck Institute for Meteorology Grand Ensemble (MPI-GE) members, unforced variability can explain more than 90% of the historical EP and CP El Niño standard deviation and all of the ENSO skewness spread in the 17 CMIP5 models. Both CESM-LE and the selected CMIP5 models show increased EP and CP El Niño variability in a warmer climate, driven by a stronger mean vertical temperature gradient in the upper ocean and faster surface warming of the eastern equatorial Pacific. However, MPI-GE shows no agreement in EP or CP standard deviation change. This is due to weaker sensitivity to the warming signal, such that when the eastern equatorial Pacific surface warming is faster, the change in upper ocean vertical temperature gradient tends to be weaker. This highlights that individual models produce a different ENSO response in a warmer climate, and that considerable uncertainty within the CMIP5 ensemble may be caused by internal climate variability.

KEYWORDS: El Niño; ENSO; Climate change; Tropical variability

1. Introduction

El Niño–Southern Oscillation (ENSO) is the leading mode of interannual variability across the globe, generating severe weather events which impact agriculture and ecosystems (Aronson et al. 2000; Glynn and de Weerdt 1991; Vincent et al. 2011). As a diverse and dynamic phenomenon, it is widely accepted that there are at least two types of El Niño events: the canonical eastern Pacific (EP) and central Pacific (CP) El Niño (Johnson 2013; Capotondi et al. 2015). EP El Niño tends to be stronger than CP events, with anomalously warm sea surface temperatures (SSTs) in the central to eastern Pacific and an eastward shift of the Walker circulation. This in turn generates increased rainfall over parts of South America while dry conditions develop over the western Pacific (Chiew et al. 1998; Grimm and Tedeschi 2009; Ropelewski and Halpert 1986). The extreme 1997/98 EP El Niño event shifted the intertropical convergence zone equatorward, leading to intense rainfall over the eastern equatorial Pacific and severe flooding in parts of

Ecuador and Peru (Douglas et al. 2009). Coral bleaching related to this extreme event was observed in reefs across the Pacific while Indonesia, eastern Australia, and the Amazon basin experienced drought and bushfires (Aronson et al. 2000; Glynn et al. 2001; Siegert et al. 2001).

In contrast to EP El Niño events, CP El Niño, sometimes called warm-pool El Niño (Kug et al. 2009), El Niño Modoki (Ashok et al. 2007), or date line El Niño (Larkin and Harrison 2005), exhibits maximum warming in the central Pacific. Due to the different location of warming, the impacts, evolution, and predictability of CP El Niño differ from EP El Niño (Kao and Yu 2009; Yeh et al. 2014; Capotondi et al. 2015). CP El Niño can cause significant changes in atmospheric circulation and convection, potentially leading to increased landfall of Atlantic hurricanes (Kim et al. 2009). The extreme 2015/16 El Niño was a mixed type of event (Santoso et al. 2017) and had significant impacts across the globe. Parts of the Amazon experienced severe drought (Jiménez-Muñoz et al. 2016) while devastating coral bleaching and declines in seabird colonies were observed in the central equatorial Pacific (Brainard et al. 2018). Due to these impacts and diversity, understanding the response of ENSO to a warmer climate is a priority in climate research.

The two main EP and CP regimes represent ENSO diversity and the nonlinearity between El Niño and La Niña events (Dommenget et al. 2013; Takahashi and Dewitte 2016;

⚘ Supplemental information related to this paper is available at the Journals Online website: https://doi.org/10.1175/JCLI-D-20-0232.s1.

Corresponding author: Benjamin Ng, benjamin.ng@csiro.au

Williams and Patricola 2018). These can be described by the E-index and C-index, respectively, calculated using empirical orthogonal function (EOF) analysis of tropical Pacific SSTs (Takahashi et al. 2011). These two indices are just one of the many methods to identify ENSO diversity; other approaches include variables such as sea surface salinity, subsurface temperature, or outgoing longwave radiation (Capotondi et al. 2015). Many of these methods use spatially fixed regions, which may capture the location of maximum variability in some coupled models but not others. By using EOF analysis, each model or observational product can express its own variability and maximum center (Takahashi et al. 2011). Utilizing this method to identify models that simulate ENSO diversity, Cai et al. (2018) showed that models from phase 5 of the Coupled Model Intercomparison Project (CMIP5) project an increase in the frequency of EP El Niño under increasing greenhouse gases.

In many climate model studies (e.g., Cai et al. 2018), one experiment from a model is often used, and as such, the role of internal variability within each model in modulating the response to increasing greenhouse gases is not clear. Here, internal climate variability represents unforced natural variability and is one of the three main causes of uncertainty in climate projections, the other two being the forcings and model response (Hawkins and Sutton 2009; Deser et al. 2012). Therefore, internal climate variability can lead to large intramodel spread in projections due to the chaotic variability of a model's climate system. The importance of unforced natural variability has been highlighted by previous studies (e.g., Deser et al. 2012; Stevenson 2012) with the suggestion that ENSO's strong variability on decadal time scales may be caused by natural variability (Wittenberg 2009). This raises the issue as to whether a single experiment is representative of each model in multimodel ensemble projections. Zheng et al. (2018) analyzed the influence of internal variability on the response of ENSO amplitude (using Niño-3 SST) to increasing greenhouse gases utilizing 40 Community Earth System Model Large Ensemble members (CESM-LE; Kay et al. 2015). They showed that the uncertainty of the Niño-3 amplitude change in CESM-LE is similar in magnitude to CMIP5 models, suggesting that unforced natural variability contributes up to 80% of the CMIP5 uncertainty in the projected Niño-3 amplitude change.

Another study by Maher et al. (2018) examined the ENSO response in CESM-LE and the Max Planck Institute Grand Ensemble (MPI-GE). They found that large ensembles with at least 30–40 members are required to adequately quantify internal variability in projections of ENSO. They also noted that internal climate variability can account for up to 90% of the CMIP5 diversity, similar to Zheng et al. (2018). When comparing the large ensembles with the CMIP5 ensemble, Maher et al. (2018) and Zheng et al. (2018) only considered the Niño-3 and Niño-4 indices. As these spatially fixed indices were used, the influence of internal variability on the simulation of the two EP and CP ENSO regimes and their response to greenhouse warming remains uncertain. Using CESM-LE and MPI-GE, we investigate EP (E-index) and CP (C-index) standard deviation and skewness to understand the influence of internal

climate variability on these properties along with its contribution to the CMIP5 ensemble.

2. Data and methodology

The extent to which the EP and CP ENSO regimes are distinct is reflected in the nonlinear relationship between the two leading principal components (PCs), described by a second-order (quadratic) polynomial fit, $PC2(t) = \alpha[PC1(t)]^2 + \beta PC1 + \gamma$ (Cai et al. 2018; Dommenget et al. 2013), with alpha (α) measuring the strength of nonlinearity. Stronger (more negative) alpha tends to be associated with greater positive E-index skewness and more negative C-index skewness, allowing the contrast in SST anomaly magnitude between EP and CP ENSO types to be quantified. Cai et al. (2018) showed that the majority of CMIP5 models have an alpha value that is weaker than the 1948–2015 observed value of -0.31. Seventeen out of 34 (50%) CMIP5 models simulate an alpha value at least half of the observed (-0.155).

These 17 CMIP5 models (Table S1 in the online supplemental material) have distinct centers for the two ENSO types and were examined by Cai et al. (2018) to assess the response of E-index variability to a warmer climate. The threshold value of 50% was chosen so that as many models as possible could be analyzed while still retaining meaningful ENSO nonlinearity. Another method for model selection is to use the two standard deviation spread from CESM-LE and MPI-GE (± 0.12 and ± 0.16, respectively) and examine models that lie within this spread from the observations. This would give a selection range from -0.43 to 0.11, which includes 18 CMIP5 models and would not significantly alter our results. As such, we examine the same 17 models used by Cai et al. (2018) to provide context for the CESM-LE and MPI-GE results. Only the first realization, initialization, and physics (i.e., r1i1p1) of each CMIP5 model are used. Using all available realizations for the 17 selected models does not appear to alter the strength of the relationships observed in this analysis, but it does increase the uncertainty and spread of the CMIP5 ensemble for some properties. However, the relatively low number of CMIP5 realizations (six or fewer in this study) may not be enough as it has been suggested by Maher et al. (2018) that ensembles of at least 30 members are required to robustly capture ENSO variability.

Data from the Twentieth Century Reanalysis v2c (20CRv2c; Compo et al. 2011), European Centre for Medium-Range Weather Forecasting (ECMWF) CERA-20C (Laloyaux et al. 2018), ECMWF ERA20C (Poli et al. 2016), Extended Reconstructed SST version 3b (ERSSTv3b; Smith et al. 2008), and Hadley Centre Sea Ice and SST version 1.1 (HadISST; Rayner et al. 2003) are used to represent observations for the 1920–99 historical period. Using these three reanalysis products and two assimilated datasets as our observations, the observed ensemble average alpha value for the 1920–99 period is -0.27 ± 0.02.

Forty members from CESM-LE are examined in this study, with all simulations from CESM version 1. CESM is composed of four different models that each represent a component of the climate system. The Community Atmosphere Model

version 5 (CAM5), the Parallel Ocean Program version 2 (POP2), the Community Land Model version 4 (CLM4), and the Los Alamos Sea Ice Model (CICE) are coupled using the CESM coupler version 7 (CPL7). The first member of CESM-LE begins at 1850 using initial conditions from a randomly selected date of the preindustrial control run (1 January, year 402). Subsequent ensemble members begin from 1 January 1920 of ensemble member 1. To simulate internal climate variability, the initial condition of member 2 uses 1-day lagged ocean temperatures from member 1 and for members 3–40, small differences in the initial condition are created by small round-off differences in air temperature. Each member then evolves freely through stochastic processes and any difference between runs is therefore due to internal variability. All members of CESM-LE have the same external forcings, which follow the CMIP5 design protocol (Taylor et al. 2012); historical forcings are applied from 1850/1920 to 2005 and representative concentration pathway 8.5 (RCP8.5) forcings from 2006 to 2100. Further information about CESM-LE and its experiment design can be found in Kay et al. (2015).

Ninety-nine MPI-GE members (Maher et al. 2019) are also analyzed. MPI-GE uses the MPI Earth System Model (MPI-ESM) version 1.1.00p2 in a low-resolution setup consisting of the following components: MPI Ocean Model (MPIOM) on a GR15L40 grid, Hamburg Ocean Carbon Cycle model version 5.2 (HAMOCC5.2) for ocean biogeochemistry, ECHAM version 6.3.01p3 for the atmospheric component, and JSBACH version 3.00 for the land model. Each member of MPI-GE begins on 1 January 1850 but is initialized from the state of 1 January using different years of the control simulation. This leads to each member representing a different state of the 1850 climate system. Additional details about MPI-GE, its experiment design, and data availability can be found in Maher et al. (2019). While all 99 MPI-GE members are used in this analysis, not all of them simulate ENSO nonlinearity with only 47 members simulating an alpha value at least half of the observed. CESM-LE and MPI-GE were the only publicly available large ensembles at the time of analysis; however, more large ensembles have been released recently due to greater awareness of the uncertainty caused by internal variability (Deser et al. 2020).

Historical (1920–99) and future (2020–99) SSTs and ocean temperatures from CESM-LE, MPI-GE, and CMIP5 are regridded to a 1° × 1° grid. The future data for all three ensembles follow the high-emissions RCP8.5 trajectory. When examining future minus historical changes, the results are scaled by the global mean SST warming (defined as the future global mean SST average minus the historical global mean SST average) to account for differences in the warming rate between models and runs. Linear correlation and regression are used to identify relationships between variables. For each member of CESM-LE and MPI-GE, and each CMIP5 model, EOF analysis is conducted on quadratically detrended monthly SST anomalies over the tropical Pacific (15°S–15°N, 140°E–80°W) from 1920 to 2099. The SST anomalies used in the EOF analysis are referenced to the historical (1920–99) climatology. Another method to remove the forced signal is to remove the ensemble mean (e.g., Frankcombe et al. 2015); however, as we are also examining the CMIP5 ensemble where each model

has a different forced signal, we apply the same methodology to all three ensembles.

In both CESM-LE and MPI-GE, the leading EOF (ensemble mean) pattern represents strong warming across the equatorial Pacific and the second EOF pattern is a dipole with cold anomalies in the EP and warming in the western Pacific (Fig. S1). The associated PC time series are normalized by their respective standard deviations and then used to calculate the $E(\mathrm{PC1} - \mathrm{PC2}/\sqrt{2})$ and $C(\mathrm{PC1} + \mathrm{PC2}/\sqrt{2})$ indices, representing EP and CP El Niño events, respectively (Takahashi et al. 2011). We examine E-index and C-index standard deviation (s) and skewness—defined as the third central moment (m_3), where skewness = $(m_3/s^3) = (1/n)\sum_{i=1}^{n}(x_i - \overline{x})^3 / \left\{ [1/(n-1)]\sum_{i=1}^{n}(x_i - \overline{x})^2 \right\}^{3/2}$ —in the three ensembles and their relationship with alpha in the following section.

3. Results

a. The role of internal variability in simulating properties of two ENSO regimes

The historical CESM-LE mean SST standard deviation (Fig. 1b) is considerably stronger than observed (Fig. 1a) but the structure is comparable. The MPI-GE ensemble has a similar magnitude to observations but exhibits a double peak with warming centers in both the eastern and western equatorial Pacific (Fig. 1d). Both ensembles exhibit a westward bias that likely arises from the cold tongue bias that is common in models (Kug et al. 2012; Bellenger et al. 2014). Figures 1c and 1e show the intermember regression between historical alpha and grid point SST standard deviation for CESM-LE and MPI-GE, respectively. Both models display a basinwide negative relationship between alpha and SST standard deviation with a minimum in the central Pacific, indicating that when an ensemble member has a stronger (i.e., more negative) alpha amplitude, SST standard deviation in the central Pacific tends to be larger. However, the CESM-LE regression pattern is notably stronger and has a wider longitudinal extent compared to MPI-GE.

The intermember/intermodel relationship between alpha and E-index standard deviation is shown in Fig. 1f. CESM-LE and MPI-GE show a significant correlation (at the 95% confidence level) although the correlation for MPI-GE is weak ($R = -0.23$). The selected CMIP5 models also have a strong intermodel relationship that is significant at the 90% confidence level. For alpha and C-index standard deviation (Fig. 1g), only CESM-LE shows a significant relationship. These relationships suggest that CESM-LE members with more negative alpha tend to have stronger EP and CP El Niño events and variability, as represented by the larger E-index and C-index standard deviations. Therefore, in CESM-LE, it indicates that EP and CP ENSO amplitude is related to the strength of ENSO nonlinearity which arises from unforced natural variability. When the system is more nonlinear, El Niño events tend to be stronger in CESM-LE. Using all available realizations from the 17 CMIP5 models does not appear to alter the results (Figs. S2a,b) and a similar relationship is seen when
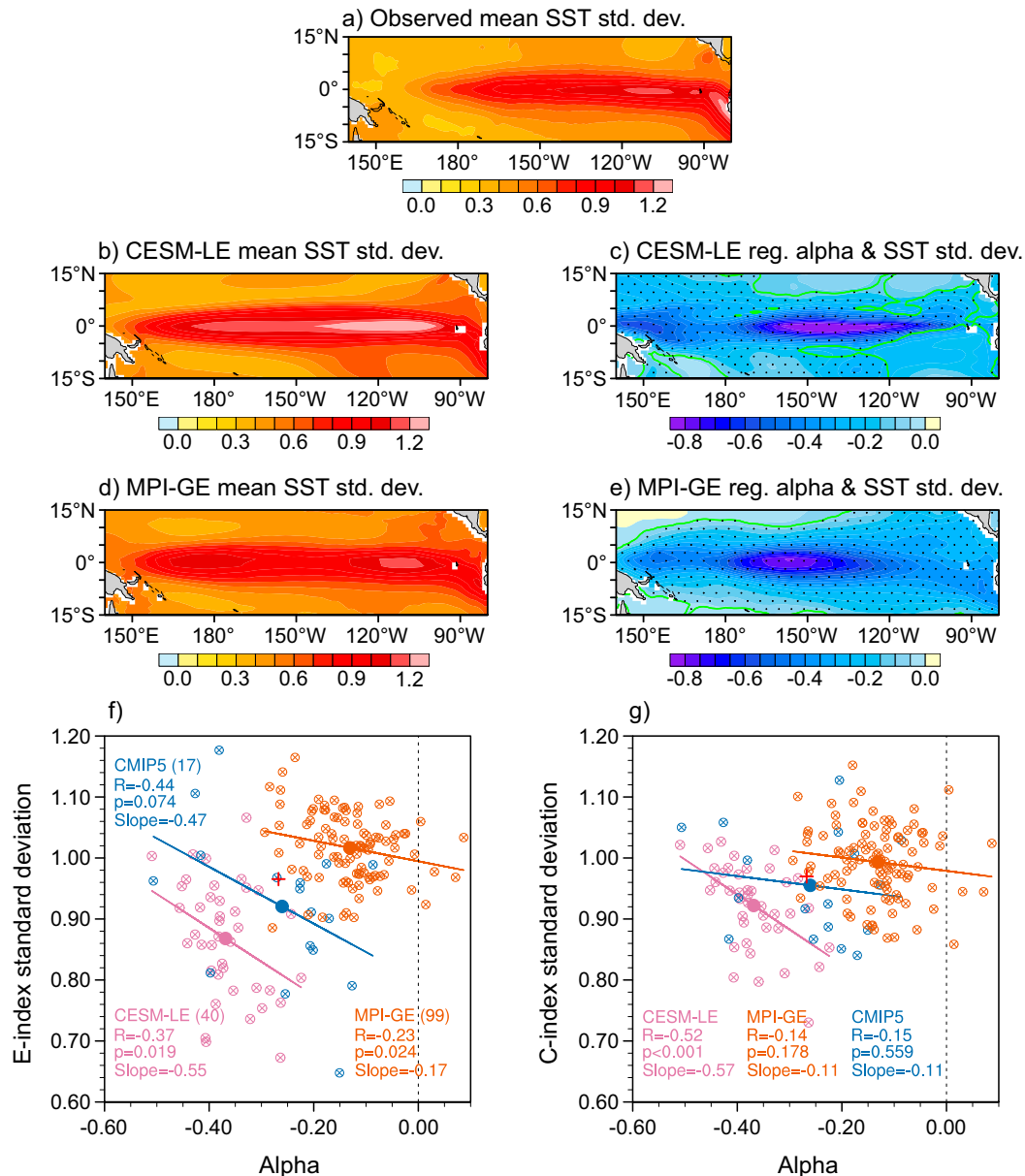
FIG. 1. (a) 1920–99 historical observed mean SST standard deviation over the tropical Pacific from five reanalysis datasets. (b) Historical CESM-LE mean SST standard deviation from 40 members. (c) CESM-LE intermember regression of grid point historical SST standard deviation onto historical alpha. (d),(e) As in (b) and (c), respectively, but for 99 MPI-GE members. (f) Relationship between historical alpha and E-index standard deviation. (g) As in (f), but for alpha and C-index standard deviation. Stippling in (c) and (e) represents regions where the intermember correlation is significant at the 95% confidence level, based on a two-tailed Student's t test. Open pink, orange, and blue circles with crosses in (f) and (g) represent CESM-LE members, MPI-GE runs, and CMIP5 models, respectively. Solid circles in (f) and (g) represent their respective ensemble means. The red plus sign in (f) and (g) represents the ensemble mean from the three reanalysis and two observational datasets.

comparing historical alpha with Niño-3 and Niño-4 standard deviation (Figs. S3a,b). This shows that SST variability over the Niño-3 and Niño-4 regions is significantly related to alpha in the three ensembles, as can be seen in Figs. 1c and 1e.

The alpha ensemble mean values can be compared to observations (Figs. 1f,g). CESM-LE simulates an ensemble mean alpha value (-0.37) that is stronger than observed (-0.27 for the 1920–99 period) while MPI-GE has a relatively weak ensemble mean alpha (-0.13). The selected CMIP5 mean alpha (-0.26) is close to the observations. These alpha values show that CESM-LE simulates both strong ENSO nonlinearity and the two distinct EP and CP ENSO regimes.
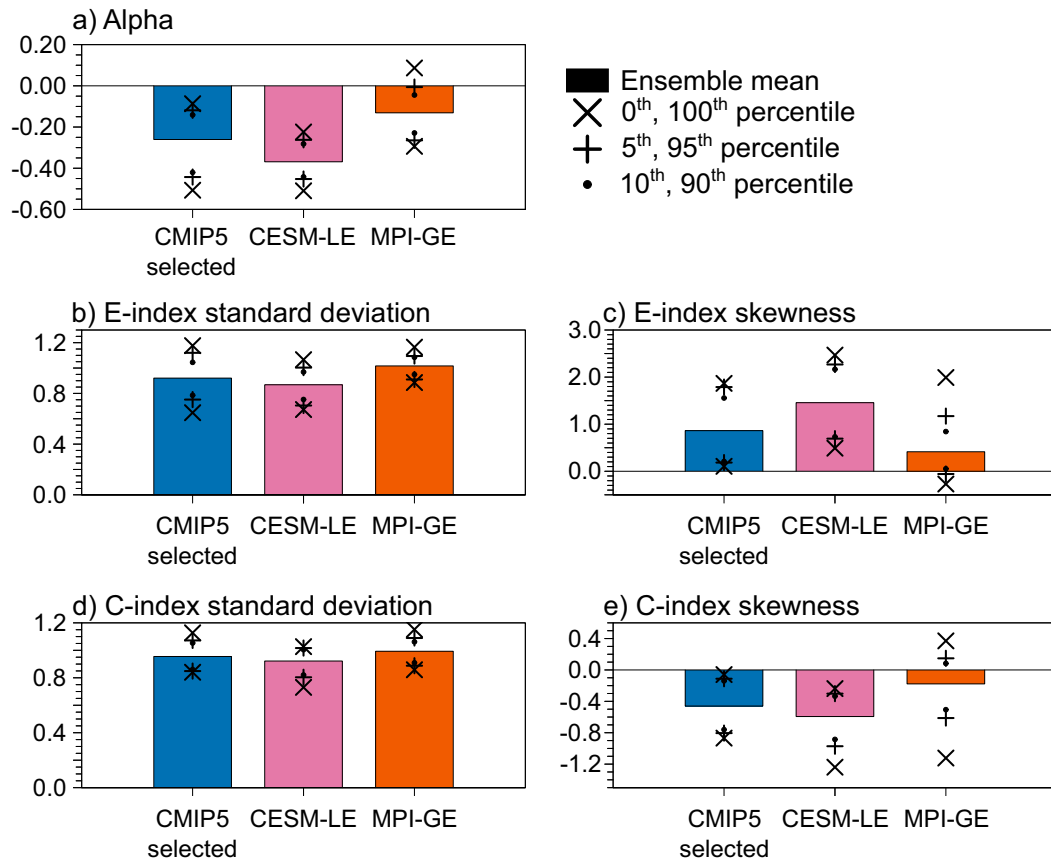
FIG. 2. (a) Historical alpha ensemble mean and percentiles for the 17 selected CMIP5 models, 40 CESM-LE, and 99 MPI-GE simulations. (b)–(e) As in (a), but for E-index standard deviation, E-index skewness, C-index standard deviation, and C-index skewness, respectively.

To quantify the role of internal variability, Fig. 2a shows the historical alpha ensemble mean along with the full range, 5th–95th, and 10th–90th percentiles for the selected CMIP5 models, CESM-LE, and MPI-GE. Following the method of Maher et al. (2018), this shows that internal climate variability may explain up to 90% of the diversity in the selected CMIP5 ensemble as the spread of CESM-LE and MPI-GE is as large as the 5th–95th percentiles of the selected CMIP5 ensemble. The intermember spread of CESM-LE and MPI-GE can explain up to 90% of the E-index uncertainty in the selected CMIP5 ensemble (Fig. 2b). Similar results also occur for the C-index with unforced natural variability accounting for 90%–100% of the C-index standard deviation diversity in the selected CMIP5 ensemble (Fig. 2d). The inclusion of all available realizations for the 17 selected CMIP5 models does not considerably affect our results (Fig. S4). This may be because of the low number of realizations available for each of the CMIP5 models.

Amplitude and spatial nonlinearity are dominant characteristics of ENSO and this leads to strong positive SST skewness over the central and eastern Pacific, while large negative SST skewness is located in the western Pacific (Capotondi et al. 2015). The positive SST skewness indicates that warm SST anomalies associated with El Niño events, tend to be stronger than cool SST anomalies in the eastern Pacific. Similarly, negative SST skewness in the western

Pacific implies that cold SST anomalies during El Niño tend to be stronger than warm SST anomalies during La Niña. CESM-LE and MPI-GE simulate positive EP SST skewness as seen in the historical ensemble mean (Figs. 3b,d) but the magnitudes are considerably weaker than observed (Fig. 3a) and also contain a westward bias. The linear regression pattern of grid-point SST skewness onto alpha is shown in Figs. 3c and 3e for CESM-LE and MPI-GE, respectively. Both models exhibit a negative relationship between alpha and SST skewness in the central to eastern Pacific, indicating that more negative alpha values are associated with a more positive SST skewness. A positive relationship is observed in the western Pacific where SST skewness is negative due to the El Niño–induced cooling in the region. Therefore, when alpha amplitude is larger (i.e., more negative), SST skewness also tends to be more negative and a significant positive relationship is exhibited.

As alpha is a measure of ENSO nonlinearity, all three ensembles display strong and significant negative correlations between historical alpha values and E-index skewness (Fig. 3f). When alpha is more negative, the E-index skewness tends to be more positive, with EP El Niño events generally larger in amplitude. The opposite occurs between alpha and C-index skewness where stronger alpha is associated with more negative skewness (Fig. 3g). This positive relationship occurs as the
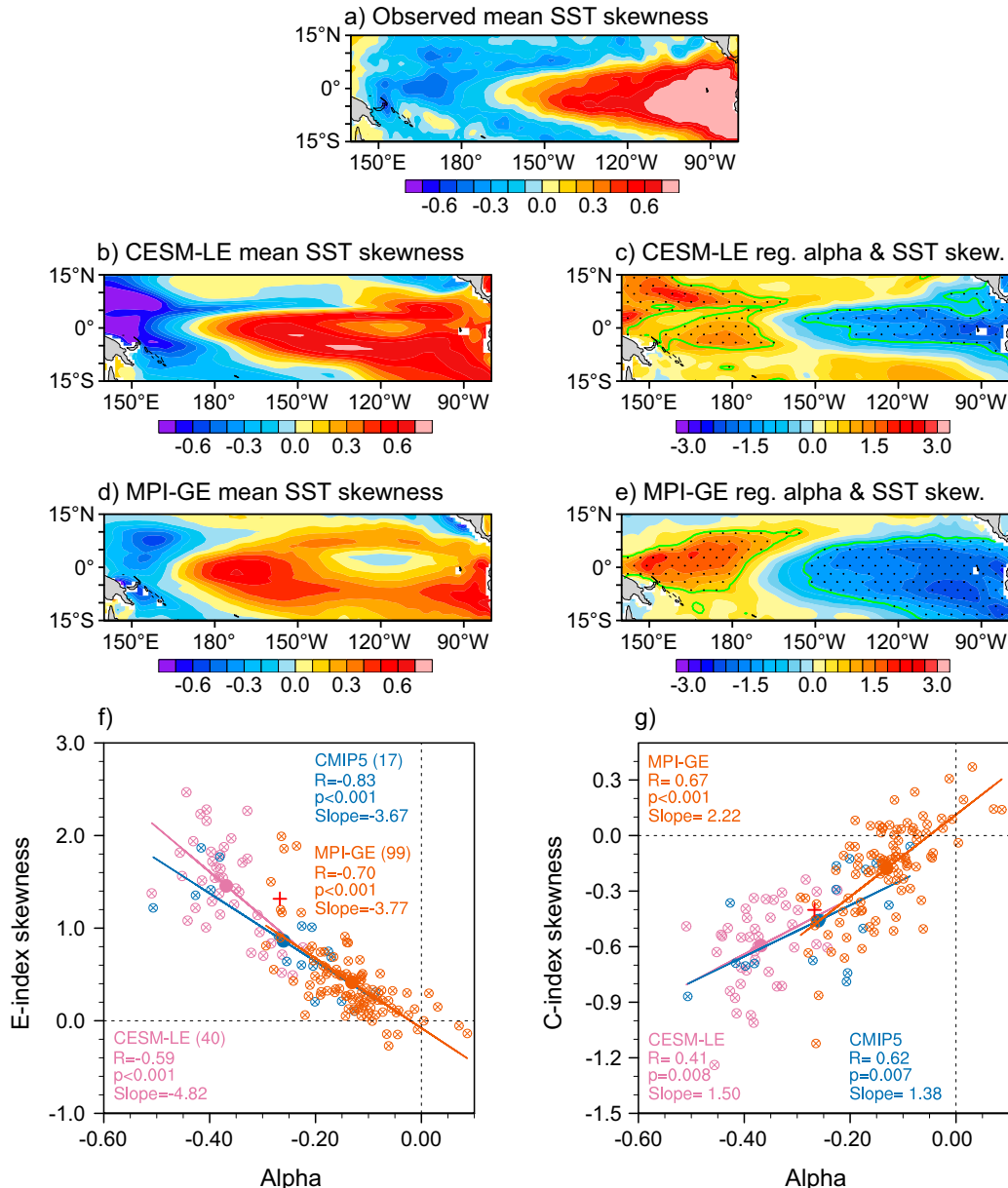
FIG. 3. (a) 1920–99 historical observed mean SST skewness over the tropical Pacific from five reanalysis datasets. (b) Historical CESM-LE mean SST skewness from 40 members. (c) CESM-LE intermember regression of grid point historical SST skewness onto historical alpha. (d),(e) As in (b) and (c), respectively, but for 99 MPI-GE members. (f) Relationship between historical alpha and E-index skewness. (g) As in (f), but for alpha and C-index skewness. Stippling in (c) and (e) represents regions where the intermember correlation is significant at the 95% confidence level, based on a two-tailed Student's *t* test. Open pink, orange, and blue circles with crosses in (f) and (g) represent CESM-LE members, MPI-GE runs, and CMIP5 models, respectively. Solid circles in (f) and (g) represent their respective ensemble means. The red plus sign in (f) and (g) represents the ensemble mean from the three reanalysis and two observational datasets.

C-index is dominated by La Niña events, which are usually stronger than CP El Niño, causing the C-index to be negatively skewed. Figures 3f and 3g clearly show that members and models with weak alpha tend to display no skewness and therefore ENSO nonlinearity in these models and members is

weak. For both E-index and C-index skewness (Figs. 2c,e), CESM-LE and MPI-GE exhibit a spread that is larger than that of the selected CMIP5 model ensemble. Therefore, unforced natural variability may account for almost all of the diversity, highlighting the importance of internal variability in
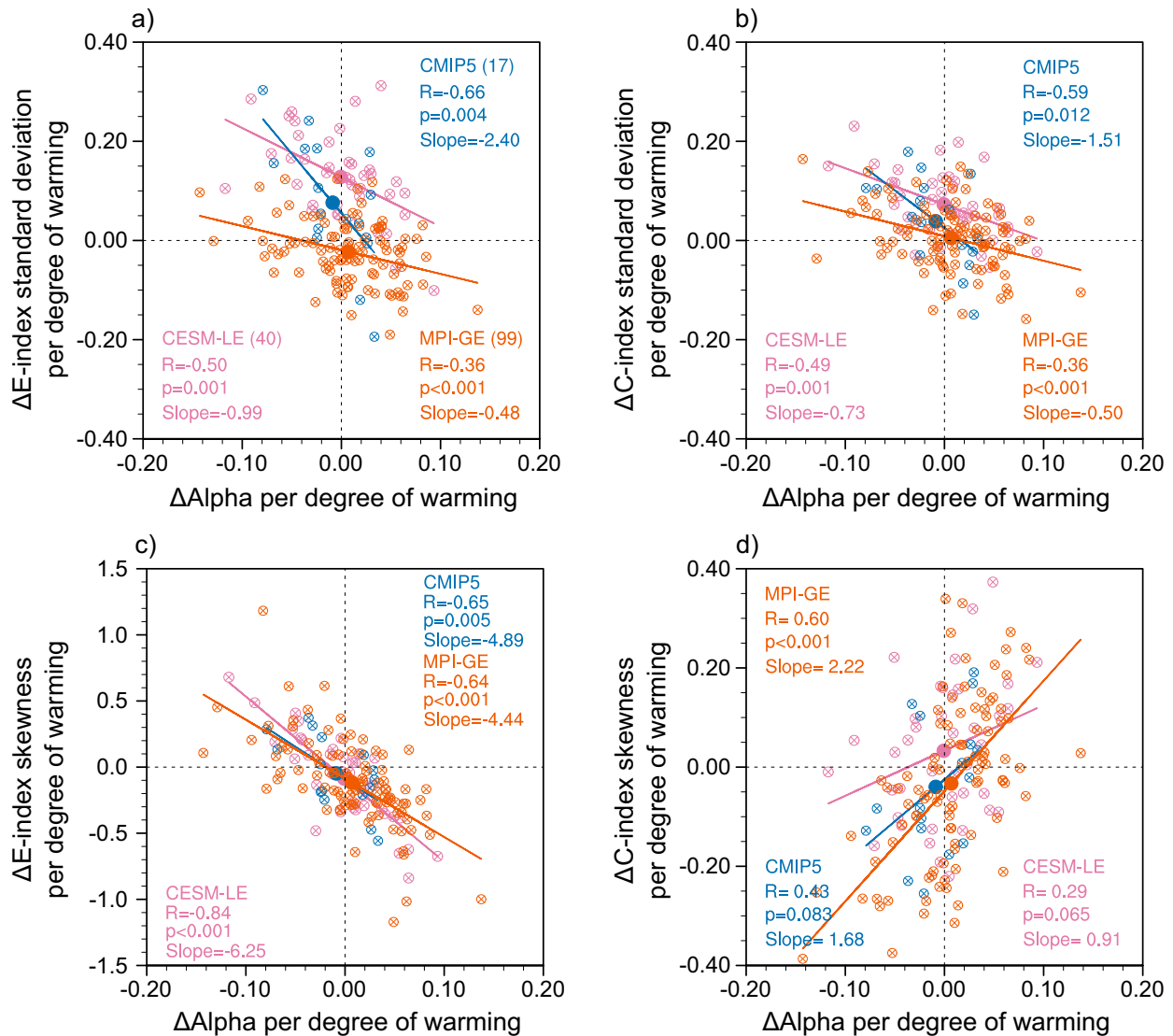
FIG. 4. (a) Relationship between future minus historical change in alpha and E-index standard deviation. (b) As in (a), but for C-index standard deviation. (c),(d) As in (a),(b), but for E-index skewness and C-index skewness, respectively. Open pink, orange, and blue circles with crosses represent CESM-LE members, MPI-GE runs, and CMIP5 models, respectively. Solid circles represent their respective ensemble means. All changes shown here have been normalized by the difference in global mean SST for each member/model and are in units of per degree of global warming.

modulating the nonlinear processes responsible for E-index and C-index skewness. The robustness of the alpha and skewness relationships are highlighted by the similar correlations when all available realizations from the 17 CMIP5 models are utilized (Figs. S2c,d). Interestingly, Niño-3 and Niño-4 skewness is not as strongly related to alpha (Figs. S3c,d) and therefore the two Niño regions may not appropriately represent ENSO nonlinearity and diversity.

b. The role of internal variability in the ENSO regimes' response to greenhouse warming

The changes (future minus historical) in alpha, E-index, and C-index statistics, and their relationships, are examined in

Fig. 4. There is a significant correlation between the changes in alpha with the changes in E-index standard deviation that occurs for all three ensembles (Fig. 4a). When alpha becomes stronger (more negative), E-index standard deviation tends to increase, suggesting that EP El Niño variability increases. The selected CMIP5 ensemble relationship is stronger than for CESM-LE and MPI-GE (e.g., compare the slope values in Fig. 4a), which suggests that while internal climate variability contributes to this relationship, there are other external forcings and model differences that may also play a role. A similar response is observed for C-index standard deviation (Fig. 4b), indicating that enhanced CP El Niño and La Niña variability are also associated with strengthened alpha.
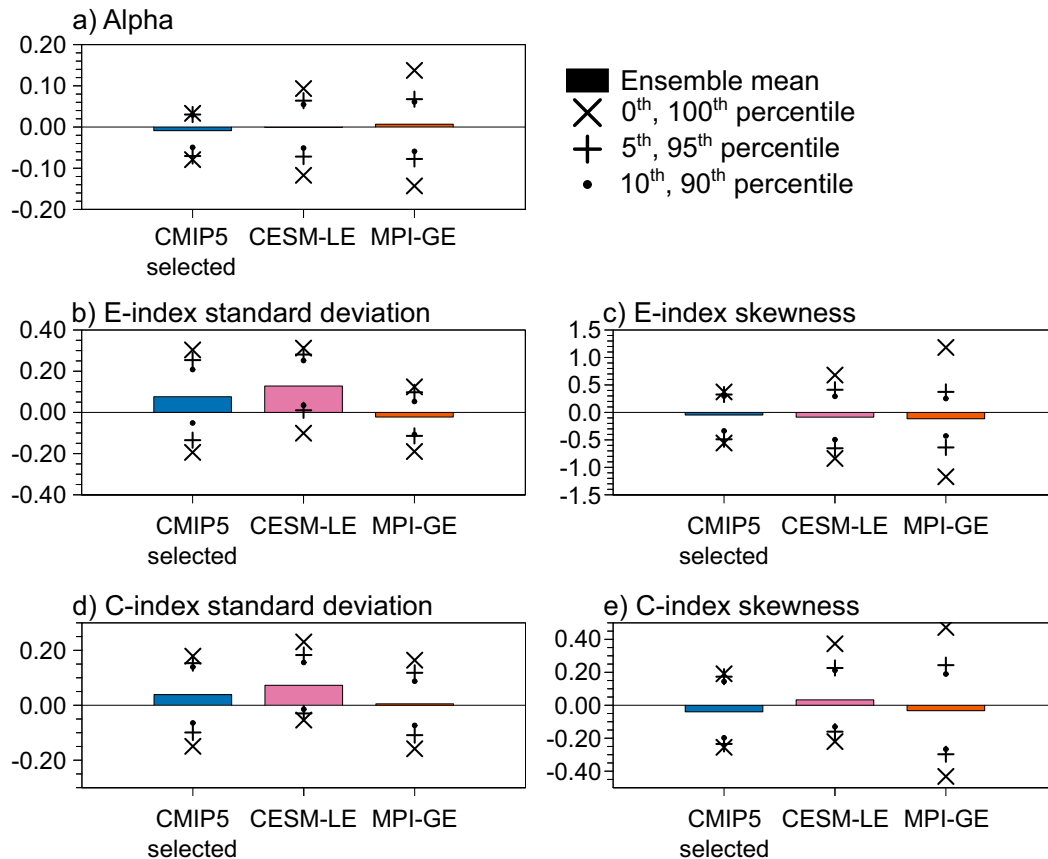
FIG. 5. (a) Future minus historical change in alpha ensemble mean and percentiles for 17 selected CMIP5 models, 40 CESM-LE, and 99 MPI-GE simulations. (b)–(e) As in (a), but for E-index standard deviation, E-index skewness, C-index standard deviation, and C-index skewness, respectively. All changes shown here have been normalized by the difference in global mean SST for each member/model and are in units of per degree of global warming.

The robustness of the projected changes in EP and CP ENSO standard deviation can be assessed by examining the consensus among models and runs. We define consensus as when 75% of an ensemble agree on the sign of the change. Both CESM-LE and CMIP5 show strong agreement in E-index standard deviation change, with 38 (95%) CESM-LE members and 14 (82%) CMIP5 models exhibiting an increase, with the latter consistent with the results of Cai et al. (2018). However, for MPI-GE only 33 (33%) members project an increase while 66 (67%) runs show a decrease in E-index standard deviation. For C-index standard deviation (Fig. 4b), 35 (88%) CESM-LE runs display an increase but only 11 (65%) CMIP5 models and 53 (54%) MPI-GE members show an increase, indicating a lack of consensus for these two ensembles.

Changes in alpha are also related to changes in E-index skewness (Fig. 4c), with a strong negative correlation for all three ensembles. Future strengthening of alpha tends to be associated with increased E-index skewness, suggesting that EP El Niño events are becoming stronger and/or occurring more frequently in the future period. The relationship between changes in alpha and C-index skewness is less clear (Fig. 4d). Only MPI-GE shows a significant relationship (at the 95%

confidence level) whereas for CESM-LE and the selected CMIP5 models the correlations are weaker and only significant at the 90% confidence level.

There is no agreement on the sign of the change in alpha. Nineteen (48%) CESM-LE runs, 9 (53%) CMIP5 models, and 38 (38%) MPI-GE members project a future strengthening of alpha (Fig. 4a). As alpha, E-index skewness, and C-index skewness are linked, there is also no consensus on the sign of E-index skewness change or C-index skewness change. Eighteen (45%) CESM-LE members and 7 (41%) CMIP5 models exhibit an increase while 70 (70%) MPI-GE runs show a decrease in future E-index skewness. For C-index skewness, 18 (45%) CESM-LE runs, 56 (56%) MPI-GE members, and 10 (59%) CMIP5 models simulate a future (more negative) increase. This lack of consensus in alpha, E-index skewness, and C-index skewness shows that the response of ENSO nonlinearity to a warmer climate is uncertain and internal variability may contribute considerably to the spread in CMIP5 models. It may also suggest that some models project a decrease in alpha and ENSO skewness, meaning that intermodel physics may play a role in addition to internal variability.

Figure 5 examines the contribution of internal climate variability to the projected model changes in alpha and E-index and C-index properties. Both CESM-LE and MPI-GE exhibit a larger spread in alpha change than the selected CMIP5 models (Fig. 5a). This shows that internal climate variability can explain all of the diversity in projected alpha changes in CMIP5. For E-index and C-index standard deviation, internal variability can explain approximately 90% and 100% of the spread, respectively (Figs. 5b,d). Similar to changes in alpha, internal variability may also explain all of the projected changes in E-index and C-index skewness (Figs. 5c,e). Therefore, the contribution of internal variability to changes in EP and CP ENSO properties is substantial and this may contribute to the uncertainty of CMIP5 projections.

c. Mechanisms of increased eastern Pacific El Niño variability and the role of internal variability

When aggregated across CMIP5 models that simulate ENSO nonlinearity, there are two main mechanisms that contribute to the increase in EP El Niño standard deviation (Cai et al. 2018). One mechanism is the faster SST warming in the equatorial eastern Pacific than the surrounding regions and in CMIP5 models; this faster warming facilitates more frequent convection, enabling the development of EP El Niño events (Cai et al. 2014). This is measured by calculating the "SST warming pattern intensity" for each member where the equatorial Pacific (5°S–5°N, 140°E–80°W) warming pattern from each member is linearly regressed onto the ensemble mean warming pattern. A larger regression coefficient (i.e., stronger SST warming pattern intensity) implies that an ensemble member has a stronger SST warming than the ensemble mean or that the warming pattern closely resembles the ensemble mean (Fig. 6a; see also Figs. S5a,c,e). The change in mean SST between the top and bottom 25% of members and models with strong/weak SST warming pattern intensity is compared in Fig. S6. The top and bottom CESM-LE members generally have spatially similar patterns, with stronger or weaker warming relative to their ensemble mean and similar behavior is seen for MPI-GE (Figs. S6a–f). For CMIP5, the four models with the weakest change in mean SST (Fig. S6g) have both weaker warming and a spatial structure (e.g., a double warming peak across the equatorial Pacific) that does not resemble the CMIP5 ensemble mean (Fig. S6i). Other studies (e.g., Zheng et al. 2016; Zheng 2019) have used Niño-3 SST relative to the tropical mean to represent the SST warming pattern. This also displays a similar relationship with E-index and C-index standard deviation changes (not shown).

As shown in Cai et al. (2018), the second and primary cause of increased EP El Niño standard deviation in CMIP5 models is increased vertical stratification of the upper ocean (Fig. 6c; Figs. S5b,d,f). Increased vertical stratification of the upper ocean allows for stronger atmosphere–ocean coupling at the wind anomaly center (Dewitte et al. 1999, 2009; An and Jin 2001; Cai et al. 2018). This in turn increases the likelihood of stochastic forcing such as westerly wind bursts triggering an EP El Niño event (Levine et al. 2016). These two mechanisms, increased stratification and relative SST warming in the eastern equatorial Pacific, are examined in CESM-LE and MPI-GE to assess whether internal variability affects the relationship of these two processes with respect to the change in E-index and C-index standard deviation.

In a warmer climate, CMIP5 models with a stronger SST warming pattern intensity (Fig. S6h) tend to project a larger increase in E-index standard deviation (Figs. 6a,b), in agreement with Cai et al. (2018). A similar response is also observed for CESM-LE; however, there is no correlation among MPI-GE members. This lack of agreement between the two large ensembles increases uncertainty about the relationship between SST warming pattern intensity and the change in E-index standard deviation. However, as more large ensembles from different models become available, an intermodel relationship may become clearer.

Selected CMIP5 models and MPI-GE runs show no relationship between SST warming pattern intensity and the change in C-index standard deviation (Fig. 6b). This indicates that the sensitivity of CP El Niño or La Niña to eastern equatorial Pacific warming may be weaker in these two ensembles. Other compensating factors may also be at play; for example, the different warming patterns between CMIP5 models suggest that some members have a warming maximum in the eastern Pacific whereas other models have a double-peak warming pattern (Figs. S6g–i). MPI-GE's SST variability also features a double-peak pattern (Fig. 1d) and an SST warming pattern intensity that is relatively weaker (Figs. S5h and S6d–f). These differences may act to offset or weaken the intermodel/intermember relationship. CESM-LE, however, exhibits a significant correlation, which may arise because of the significant positive correlation between E-index standard deviation and C-index standard deviation (Fig. S7) and E-index standard deviation and SST warming pattern intensity (Fig. 6a). When a CESM-LE member has large EP El Niño variability, CP El Niño variability also tends to be large and a La Niña event tends to follow a strong El Niño (Figs. S7 and S8; Cai et al. 2015). Although MPI-GE also displays a significant historical relationship between C-index standard deviation and E-index standard deviation (Fig. S7a), the correlation is not very strong ($R = 0.37$) and there is large uncertainty.

The change in mean vertical temperature gradient of the upper ocean, defined as the difference between the mean temperature over the upper 75 m and the temperature at 100 m averaged over 5°S–5°N, 150°E–140°W, shows significant correlations with E-index standard deviation change for all three ensembles (Fig. 6c). As in Cai et al. (2018), changes in the mean vertical temperature gradient can explain approximately 55% ($R^2 = 0.55$) of the change in E-index standard deviation for the selected CMIP5 models. This contribution from mean vertical temperature gradient changes is stronger than that from SST warming pattern intensity ($R^2 = 0.40$) and similar behavior occurs for MPI-GE [i.e., compare the CMIP5 and MPI-GE correlation coefficients in Figs. 6a and 6c; see also Cai et al. (2018), their Fig. 3]. These stronger correlations in MPI-GE and the selected CMIP5 models suggest that changes in the mean vertical temperature gradient play a larger role in the response of EP ENSO standard deviation to a warmer climate. In contrast, SST warming pattern intensity and faster warming of the eastern equatorial Pacific appears to play a larger role in E-index standard deviation changes of CESM-LE as the relationship between the mean vertical temperature gradient and E-index standard deviation is relatively weaker (i.e.,
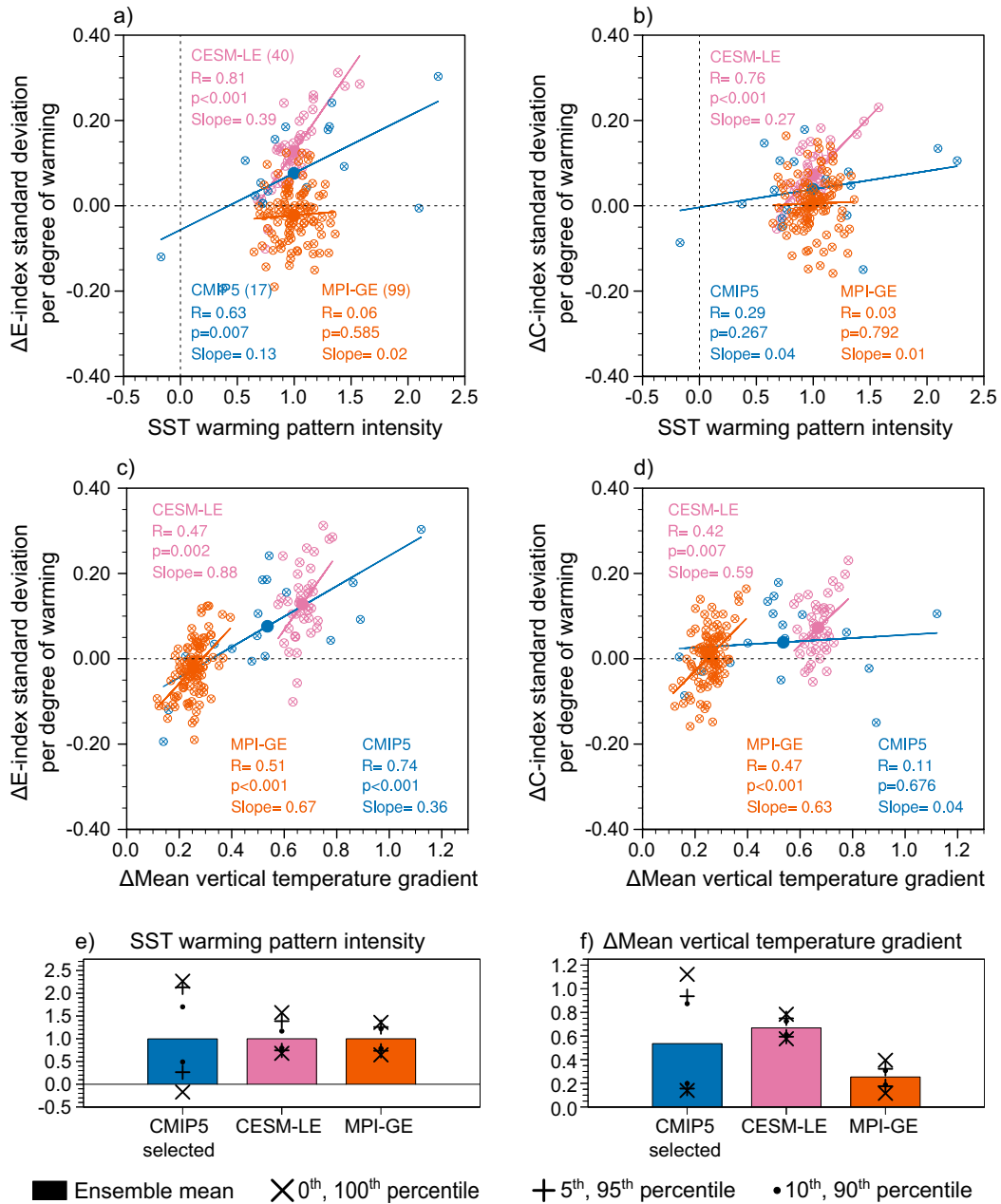
FIG. 6. (a) Relationship between SST warming pattern intensity and change in E-index standard deviation. (b) As in (a), but for the change in C-index standard deviation. (c) Relationship between the change in upper ocean mean vertical temperature gradient and the change in E-index standard deviation. (d) As in (c), but for the change in C-index standard deviation. (e) Intermember spread and percentiles of SST warming pattern intensity for selected CMIP5 models, CESM-LE, and MPI-GE. (f) As in (e), but for the change in mean vertical temperature gradient. Open pink, orange, and blue circles with crosses in (a)–(d) represent CESM-LE members, MPI-GE runs, and CMIP5 models, respectively. Solid circles represent their respective ensemble means. All changes have been normalized by the difference in global mean SST for each member/model and are in units of per degree of global warming.

comparison of the correlation coefficients in Figs. 6a and 6c). Both MPI-GE and CESM-LE show a significant relationship between E-index and C-index standard deviation (Fig. S7) and thus both ensembles display significant correlations between

the change in C-index standard deviation and mean vertical temperature gradient (Fig. 6d).

The contribution of internal climate variability to SST warming pattern intensity spread in CMIP5 is at most 80%,

with the diversity of CESM-LE and MPI-GE being considerably smaller than the selected CMIP5 spread (Fig. 6e). A similar response is also seen for changes in the mean vertical temperature gradient (Fig. 6f). Diversity in CMIP5 is larger because the external forcings and the model response to these external forcings differ among CMIP5 models. Additional uncertainties are also caused by model biases, physics, and parameterizations (Kay et al. 2015; Maher et al. 2018). In contrast, both large ensembles have the same external forcing between members and the biases, physics, and parameterizations are the same in every run.

4. Discussion

It is clear that internal variability influences the response of ENSO to a warmer climate with many studies examining this relationship (e.g., Wittenberg 2009; Deser et al. 2012; Vega-Westhoff and Sriver 2017; Zheng 2019). Previous studies utilizing large ensembles have examined ENSO and internal variability using the Niño-3 and Niño-4 indices to represent ENSO (i.e., Maher et al. 2018; Zheng et al. 2018). However, the use of the E-index and C-index to capture ENSO diversity and alpha to measure nonlinearity is relatively new. As such, this study aims to build on the results of Cai et al. (2018), who showed that CMIP5 models that realistically simulate ENSO diversity project an increase in EP El Niño standard deviation in response to a warmer climate. The same CMIP5 models analyzed in Cai et al. (2018) are examined here to put the large ensemble results into context. However, in light of the recent release of CMIP6 models, it is possible that the response of this newer generation of models may be different. Climate sensitivity in CMIP6 appears to be considerably higher than that of CMIP5 (Zelinka et al. 2020). Therefore, CMIP6 models are simulating a stronger warming in response to increasing greenhouse gases, which leads to greater warming across the equatorial Pacific (Grose et al. 2020, their Fig. 8). If the results presented here were to hold, the stronger warming in CMIP6 may lead to an even larger change in E-index standard deviation but further research is needed to confirm this.

Alpha is used to measure ENSO diversity and the nonlinearity between the two leading principal components of EOF analysis over the equatorial Pacific. The relationship between alpha and ENSO nonlinearity can be seen in the strong correlation between alpha and E-index and C-index skewness (Figs. 3f,g). It is important to note, however, that alpha (and ENSO skewness) varies with respect to the period analyzed as ENSO is a dynamic and evolving phenomenon. It is clear for MPI-GE that some members exhibit an alpha value that is less than half of the observed but the cause of this is not yet understood. One possible explanation may be MPI-GE's unrealistic double peak in SST variability in the eastern and western Pacific (Fig. 1d). Nevertheless, the results presented here show that large diversity arises from internal variability, even in models that have the physics to simulate realistic alpha (e.g., CESM-LE). This diversity can influence ENSO's own response to a warmer climate, increasing our uncertainty of its projected changes (Cai et al. 2020).

There is large uncertainty as to whether ENSO skewness, as represented by the E-index, C-index, and alpha will change in a warmer climate (Figs. 4c,d). All three ensembles show no consensus despite E-index and C-index standard deviation generally increasing. Generally, an increase in standard deviation can lead to stronger skewness but the results show that larger standard deviation changes tend to be associated with larger changes in the mean state (i.e., upper ocean stratification and eastern equatorial Pacific SST warming; Fig. 6). Therefore, the lack of agreement may be caused by how skewness is calculated, where it is referenced to a changing mean, potentially leading to a two-way interaction between mean state change and ENSO skewness.

As mentioned in section 3b, there is no agreement between MPI-GE members on how EP or CP El Niño variability responds to a warmer climate (Figs. 4–6). This may be caused by the comparatively weaker warming along the equatorial Pacific in MPI-GE (Fig. S5c) than in CESM-LE or CMIP5 (Figs. S5a,e). This relatively weaker warming is clear when the SST warming pattern is referenced to the ensemble mean using all 17 CMIP5, 99 MPI-GE, and 40 CESM-LE members (Fig. S5h). Similarly, MPI-GE's change in ocean temperature and upper-ocean stratification along the equator is also relatively weaker than CESM-LE and CMIP5 (Figs. 6c,d; Figs. S5b,d,f). The relationship between the SST warming pattern intensity (relative to each ensemble's own mean) and the change in mean vertical temperature gradient in MPI-GE is opposite to CESM-LE and CMIP5 (Fig. S5g). This weaker upper-ocean stratification change, combined with the opposite relationship between the two processes, suggests that MPI-GE's ocean–atmosphere coupling may be relatively weaker. Further examination of this is required but a weaker coupling between the atmosphere and ocean could explain the uncertain response of E-index and C-index standard deviation to increasing greenhouse gases in MPI-GE. This highlights that individual models have a different response of ENSO to a warmer climate which may be influenced by biases and parameterizations unique to each model.

5. Conclusions

The influence of internal climate variability on EP (E-index) and CP (C-index) El Niño standard deviation and skewness are examined using two large model ensembles, CESM-LE and MPI-GE. Seventeen selected CMIP5 models that simulate ENSO nonlinearity were also analyzed to approximate the contribution of natural variability to the CMIP5 ensemble. In the historical (1920–99) period, internal variability may account for between 90% and 100% of E-index standard deviation and skewness diversity among the 17 selected CMIP5 models. A similar proportion (90%–100%) of C-index standard deviation and skewness spread is also explained by internal variability. This shows that unforced natural variability of the climate system is a large source of uncertainty in CMIP5 EP and CP El Niño properties. Although different indices (e.g., Niño-3 and Niño-4) were utilized by Maher et al. (2018) and Zheng et al. (2018), the general agreement between studies highlights that there is a consistent contribution of internal

variability to ENSO uncertainty. Future (2020–99) minus historical changes in E-index and C-index standard deviation and skewness are also examined. Although CESM-LE and CMIP5 models agree that E-index standard deviation will increase in a warmer climate, MPI-GE shows no consensus. The differing response between the two large ensembles shows that each model has its own unique response of ENSO to increasing greenhouse gases. For all four ENSO properties, the contribution of unforced natural variability to the CMIP5 ensemble is more than 90% and this increases the uncertainty of projections for these ENSO properties.

Finally, the two main mechanisms responsible for increasing EP El Niño standard deviation were examined. These mechanisms are 1) faster warming of the eastern equatorial Pacific than the surrounding regions and 2) increased stratification of the upper ocean mean vertical temperature gradient (Cai et al. 2018). These two processes are driven by increasing greenhouse gases and therefore the spread in the two large ensembles is relatively small when compared to CMIP5. As each CMIP5 model has different physics, parameterizations, and biases, their response to a warmer climate can differ vastly whereas each large ensemble member has the same configuration.

For both processes, the CMIP5 spread appears to be largely caused by differences between models and this may dominate or mask the contribution of unforced natural variability. Climate sensitivity, parameterizations, and aerosol schemes differ between CMIP5 models whereas they are the same among the large ensemble members. Another possibility is that internal variability in the CMIP5 ensemble is undersampled due to the lack of large ensembles for each model. The difference between the two large ensembles suggests that CESM-LE is more sensitive to the warming signal than MPI-GE. In CESM-LE, stronger eastern equatorial Pacific warming than the surrounding area leads to the significant relationship between the SST warming pattern intensity and the change in E-index and C-index standard deviation. In contrast, both the mean vertical temperature gradient change and SST warming pattern are relatively weaker in MPI-GE. The relationship between these two processes is weak in MPI-GE, causing the two processes to offset each other. This may explain the lack of consensus for changes in E-index and C-index standard deviation in MPI-GE.

The results presented here show that unforced natural climate variability contributes to a large proportion of the spread in ENSO properties in the CMIP5 ensemble. Therefore, future studies of ENSO projections should utilize large ensembles wherever possible to reduce the uncertainty associated with internal variability. This would lead to increased confidence in future projections.

REFERENCES

An, S.-I., and F.-F. Jin, 2001: Collective role of thermocline and zonal advective feedbacks in the ENSO mode. *J. Climate*, **14**, 3421–3432, https://doi.org/10.1175/1520-0442(2001)014<3421:CROTAZ>2.0.CO;2.

Aronson, R. B., W. F. Precht, I. G. Macintyre, and T. J. T. Murdoch, 2000: Coral bleach-out in Belize. *Nature*, **405**, 36, https://doi.org/10.1038/35011132.

Ashok, K., S. K. Behera, S. A. Rao, H. Weng, and T. Yamagata, 2007: El Niño Modoki and its possible teleconnection. *J. Geophys. Res.*, **112**, C11007, https://doi.org/10.1029/2006JC003798.

Bellenger, H., E. Guilyardi, J. Leloup, M. Lengaigne, and J. Vialard, 2014: ENSO representation in climate models: From CMIP3 to CMIP5. *Climate Dyn.*, **42**, 1999–2018, https://doi.org/10.1007/s00382-013-1783-z.

Brainard, R. E., and Coauthors, 2018: Ecological impacts of the 2015/16 El Niño in the central equatorial Pacific. *Bull. Amer. Meteor. Soc.*, **99** (1), S21–S26, https://doi.org/10.1175/BAMS-D-17-0128.1.

Cai, W., and Coauthors, 2014: Increasing frequency of extreme El Niño events due to greenhouse warming. *Nat. Climate Change*, **4**, 111–116, https://doi.org/10.1038/nclimate2100.

——, and Coauthors, 2015: ENSO and greenhouse warming. *Nat. Climate Change*, **5**, 849–859, https://doi.org/10.1038/nclimate2743.

——, and Coauthors, 2018: Increased variability of eastern Pacific El Niño under greenhouse warming. *Nature*, **564**, 201–206, https://doi.org/10.1038/s41586-018-0776-9.

——, B. Ng, T. Geng, L. Wu, A. Santoso, and M. J. McPhaden, 2020: Butterfly effect and a self-modulating El Niño response to global warming. *Nature*, **585**, 68–73, https://doi.org/10.1038/s41586-020-2641-x.

Capotondi, A., and Coauthors, 2015: Understanding ENSO diversity. *Bull. Amer. Meteor. Soc.*, **96**, 921–938, https://doi.org/10.1175/BAMS-D-13-00117.1.

Chiew, F. H. S., T. C. Piechota, J. A. Dracup, and T. A. McMahon, 1998: El Niño/Southern Oscillation and Australian rainfall, streamflow and drought: Links and potential for forecasting. *J. Hydrol.*, **204**, 138–149, https://doi.org/10.1016/S0022-1694(97)00121-2.

Compo, G. P., and Coauthors, 2011: The Twentieth Century Reanalysis Project. *Quart. J. Roy. Meteor. Soc.*, **137**, 1–28, https://doi.org/10.1002/qj.776.

Deser, C., A. Phillips, V. Bourdette, and H. Teng, 2012: Uncertainty in climate change projections: The role of internal variability. *Climate Dyn.*, **38**, 527–546, https://doi.org/10.1007/s00382-010-0977-x.

——, and Coauthors, 2020: Insights from Earth system model initial-condition large ensembles and future prospects. *Nat. Climate Change*, **10**, 277–286, https://doi.org/10.1038/s41558-020-0731-2.

Dewitte, B., G. Reverdin, and C. Maes, 1999: Vertical structure of an OGCM simulation of the equatorial Pacific Ocean in 1985–94. *J. Phys. Oceanogr.*, **29**, 1542–1570, https://doi.org/10.1175/1520-0485(1999)029<1542:VSOAOS>2.0.CO;2.

——, S. Thual, S. Yeh, S. An, B. Moon, and B. S. Giese, 2009: Low-frequency variability of temperature in the vicinity of the equatorial Pacific thermocline in SODA: Role of equatorial wave dynamics and ENSO asymmetry. *J. Climate*, **22**, 5783–5795, https://doi.org/10.1175/2009JCLI2764.1.

Dommenget, D., T. Bayr, and C. Frauen, 2013: Analysis of the non-linearity in the pattern and time evolution of El Niño Southern Oscillation. *Climate Dyn.*, **40**, 2825–2847, https://doi.org/10.1007/s00382-012-1475-0.

Douglas, M. W., J. Mejia, N. Ordinola, and J. Boustead, 2009: Synoptic variability of rainfall and cloudiness along the coasts of northern Peru and Ecuador during the 1997/98 El Niño event. *Mon. Wea. Rev.*, **137**, 116–136, https://doi.org/10.1175/2008MWR2191.1.

Frankcombe, L. M., M. H. England, M. E. Mann, and B. A. Steinman, 2015: Separating internal variability from the externally forced climate response. *J. Climate*, **28**, 8184–8202, https://doi.org/10.1175/JCLI-D-15-0069.1.

Glynn, P. W., and W. H. de Weerdt, 1991: Elimination of two reef-building hydrocorals following the 1982–83 El Niño. *Science*, **253**, 69–71, https://doi.org/10.1126/science.253.5015.69.

——, J. L. Maté, A. C. Baker, and M. O. Calderón, 2001: Coral bleaching and mortality in Panama and Ecuador during the 1997–1998 El Niño–Southern Oscillation event: Spatial/temporal patterns and comparisons with the 1982–1983 event. *Bull. Mar. Sci.*, **69**, 79–109.

Grimm, A. M., and R. G. Tedeschi, 2009: ENSO and extreme rainfall events in South America. *J. Climate*, **22**, 1589–1609, https://doi.org/10.1175/2008JCLI2429.1.

Grose, M. R., and Coauthors, 2020: Insights from CMIP6 for Australia's future climate. *Earth's Future*, **8**, e2019EF001469, https://doi.org/10.1029/2019EF001469.

Hawkins, E., and R. Sutton, 2009: The potential to narrow uncertainty in regional climate predictions. *Bull. Amer. Meteor. Soc.*, **90**, 1095–1108, https://doi.org/10.1175/2009BAMS2607.1.

Jiménez-Muñoz, J. C., C. Mattar, J. Barichivich, A. Santamaría-Artigas, K. Takahashi, Y. Malhi, J. A. Sobrino, and G. van der Schrier, 2016: Record-breaking warming and extreme drought in the Amazon rainforest during the course of El Niño 2015–2016. *Sci. Rep.*, **6**, 33130, https://doi.org/10.1038/srep33130.

Johnson, N. C., 2013: How many ENSO flavors can we distinguish? *J. Climate*, **26**, 4816–4827, https://doi.org/10.1175/JCLI-D-12-00649.1.

Kao, H.-Y., and J.-Y. Yu, 2009: Contrasting eastern-Pacific and central-Pacific types of ENSO. *J. Climate*, **22**, 615–632, https://doi.org/10.1175/2008JCLI2309.1.

Kay, J. E., and Coauthors, 2015: The Community Earth System Model (CESM) large ensemble project: A community resource for studying climate change in the presence of internal climate variability. *Bull. Amer. Meteor. Soc.*, **96**, 1333–1349, https://doi.org/10.1175/BAMS-D-13-00255.1.

Kim, H.-M., P. J. Webster, and J. A. Curry, 2009: Impact of shifting patterns of Pacific Ocean warming on North Atlantic tropical cyclones. *Science*, **325**, 77–80, https://doi.org/10.1126/science.1174062.

Kug, J.-S., F.-F. Jin, and S.-I. An, 2009: Two types of El Niño Events: Cold tongue El Niño and warm pool El Niño. *J. Climate*, **22**, 1499–1515, https://doi.org/10.1175/2008JCLI2624.1.

——, Y.-G. Ham, J.-Y. Lee, and F.-F. Jin, 2012: Improved simulation of two types of El Niño in CMIP5 models. *Environ. Res. Lett.*, **7**, 034002, https://doi.org/10.1088/1748-9326/7/3/034002.

Laloyaux, P., and Coauthors, 2018: CERA-20C: A coupled reanalysis of the twentieth century. *J. Adv. Model. Earth Syst.*, **10**, 1172–1195, https://doi.org/10.1029/2018MS001273.

Larkin, N. K., and D.E. Harrison, 2005: On the definition of El Niño and associated seasonal average U.S. weather anomalies. *Geophys. Res. Lett.*, **32**, L13705, https://doi.org/10.1029/2005GL022738.

Levine, A., F. F. Jin, and M. J. McPhaden, 2016: Extreme noise–extreme El Niño: How state-dependent noise forcing creates El Niño–La Niña asymmetry. *J. Climate*, **29**, 5483–5499, https://doi.org/10.1175/JCLI-D-16-0091.1.

Maher, N., D. Matei, S. Milinski, and J. Marotzke, 2018: ENSO change in climate projections: Forced response or internal variability? *Geophys. Res. Lett.*, **45**, 11 390–11 398, https://doi.org/10.1029/2018GL079764.

——, and Coauthors, 2019: The Max Planck Institute Grand Ensemble: Enabling the exploration of climate system variability. *J. Adv. Model. Earth Syst.*, **11**, 2050–2069, https://doi.org/10.1029/2019MS001639.

Poli, P., and Coauthors, 2016: ERA-20C: An atmospheric reanalysis of the twentieth century. *J. Climate*, **29**, 4083–4097, https://doi.org/10.1175/JCLI-D-15-0556.1.

Rayner, N. A., D. E. Parker, E. B. Horton, C. K. Folland, L. V. Alexander, D. P. Rowell, E. C. Kent, and A. Kaplan, 2003: Global analyses of sea surface temperature, sea ice, and night marine air temperature since the late nineteenth century. *J. Geophys. Res.*, **108**, 4407, https://doi.org/10.1029/2002JD002670.

Ropelewski, C. F., and M. S. Halpert, 1986: North American precipitation and temperature patterns associated with the El Niño/Southern Oscillation (ENSO). *Mon. Wea. Rev.*, **114**, 2352–2362, https://doi.org/10.1175/1520-0493(1986)114<2352:NAPATP>2.0.CO;2.

Santoso, A., M. J. McPhaden, and W. Cai, 2017: The defining characteristics of ENSO extremes and the strong 2015/2016 El Niño. *Rev. Geophys.*, **55**, 1079–1129, https://doi.org/10.1002/2017RG000560.

Siegert, F., G. Ruecker, A. Hinrichs, and A. A. Hoffmann, 2001: Increased damage from fires in logged forests during droughts caused by El Niño. *Nature*, **414**, 437–440, https://doi.org/10.1038/35106547.

Smith, T. M., R. W. Reynolds, T. C. Peterson, and J. Lawrimore, 2008: Improvements to NOAA's historical merged land–ocean surface temperature analysis (1880–2006). *J. Climate*, **21**, 2283–2296, https://doi.org/10.1175/2007JCLI2100.1.

Stevenson, S. L., 2012: Significant changes to ENSO strength and impacts in the twenty-first century: Results from CMIP5. *Geophys. Res. Lett.*, **39**, L17703, https://doi.org/10.1029/2012GL052759.

Takahashi, K., and B. Dewitte, 2016: Strong and moderate nonlinear El Niño regimes. *Climate Dyn.*, **46**, 1627–1645, https://doi.org/10.1007/s00382-015-2665-3.

——, A. Montecinos, K. Goubanova, and B. Dewitte, 2011: ENSO regimes: Reinterpreting the canonical and Modoki El Niño. *Geophys. Res. Lett.*, **38**, L10704, https://doi.org/10.1029/2011GL047364.

Taylor, K. E., R. J. Stouffer, and G. A. Meehl, 2012: An overview of CMIP5 and the experiment design. *Bull. Amer. Meteor. Soc.*, **93**, 485–498, https://doi.org/10.1175/BAMS-D-11-00094.1.

Vega-Westhoff, B., and R. L. Sriver, 2017: Analysis of ENSO's response to unforced variability and anthropogenic forcing using CESM. *Sci. Rep.*, **7**, 18047, https://doi.org/10.1038/s41598-017-18459-8.

Vincent, E. M., M. Lengaigne, C. E. Menkes, N. C. Jourdain, P. Marchesiello, and G. Madec, 2011: Interannual variability of the South Pacific Convergence Zone and implications for tropical cyclone genesis. *Climate Dyn.*, **36**, 1881–1896, https://doi.org/10.1007/s00382-009-0716-3.

Williams, I. N., and C. M. Patricola, 2018: Diversity of ENSO events unified by convective threshold sea surface temperature: A nonlinear ENSO index. *Geophys. Res. Lett.*, **45**, 9236–9244, https://doi.org/10.1029/2018GL079203.

Wittenberg, A. T., 2009: Are historical records sufficient to constrain ENSO simulations? *Geophys. Res. Lett.*, **36**, L12702, https://doi.org/10.1029/2009GL038710.

Yeh, S.-W., J.-S. Kug, and S.-I. An, 2014: Recent progress on two types of El Niño: Observations, dynamics, and future changes. *Asia-Pac. J. Atmos. Sci.*, **50**, 69–81, https://doi.org/10.1007/s13143-014-0028-3.

Zelinka, M. D., T. A. Myers, D. T. McCoy, S. Po-Chedley, P. M. Caldwell, P. Ceppi, S. A. Klein, and K. E. Taylor, 2020: Causes of higher climate sensitivity in CMIP6 models. *Geophys. Res. Lett.*, **47**, e2019GL085782, https://doi.org/10.1029/2019GL085782.

Zheng, X.-T., 2019: Indo-Pacific climate modes in warming climate: Consensus and uncertainty across model projections. *Curr. Climate Change Rep.*, **5**, 308–321, https://doi.org/10.1007/s40641-019-00152-9.

——, S.-P. Xie, L.-H. Lv, and Z.-Q. Zhou, 2016: Inter-model uncertainty in ENSO amplitude change tied to Pacific Ocean warming pattern. *J. Climate*, **29**, 7265–7279, https://doi.org/10.1175/JCLI-D-16-0039.1.

——, C. Hui, and S.-W. Yeh, 2018: Response of ENSO amplitude to global warming in CESM large ensemble: Uncertainty due to internal variability. *Climate Dyn.*, **50**, 4019–4035, https://doi.org/10.1007/s00382-017-3859-7.